Electronic Supplementary Material (ESI) for New Journal of Chemistry.

SUPPLEMENTARY INFORMATION

A smart supramolecular device for the detection of t,t-muconic acid in urine

Daniele Merli, Sonia La Cognata, Federica Balduzzi, Ana Miljkovic,
Lucio Toma, Valeria Amendola*[a]

[a] *Department of Chemistry, Università degli Studi di Pavia, via Taramelli 12, Pavia (Italy); e-mail: amendola@unipv.it*

Index:

1. Experimental

The human urine samples employed for this work were from voluntary individuals, and informed consent was obtained for any experimentation. The study was performed in compliance with the relevant laws and with the approval of our Institutional Committee.

1.1 Preparation of artificial urine

For the study reported in the manuscript, Fig. 4 (see white symbols), artificial urine was prepared following the method described by Brooks et al.[1] Components and their concentration are reported in Table S1. The solution of **tt-MA,** employed in the titration of the chemosensing ensemble (in HEPES, 0.05M pH 7), was prepared using artificial urine A), which also contained two possible interferents, i.e. citric and lactic acids. The effect of these components on the emission of the chemosensing ensemble was investigated using the artificial urines B) and C), see Table S1.

Table S1. Composition of artificial urines: sample A) contained both citric and lactic acids, while B) and C) contained either citric or lactic acid, respectively.

Component	**Concentration**	**Type of artificial urine**
Citric acid	2 mM	A) and B)
Lactic acid	1.1 mM	A) and C)
Sodium chloride	90 mM	A), B) and C)
Ammonium chloride	25 mM	A), B) and C)
L-glutamine	2 mM	A), B) and C)
Urea	170 mM	A), B) and C)
Uric acid	0.4 mM	A), B) and C)
Creatinine	7 mM	A), B) and C)
Calcium chloride.$2H_2O$	0.25 mM	A), B) and C)
Magnesium sulphate.$7H_2O$	2 mM	A), B) and C)
Sodium sulphate.$10H_2O$	10 mM	A), B) and C)
Sodium bicarbonate	25 mM	A), B) and C)
Sodium nitrate	6 mM	A), B) and C)
Iron(II) sulphate	0.005 mM	A), B) and C)
Potassium dihydrogen phosphate	1.8 mM	A), B) and C)
Di-potassium hydrogen phosphate	1.8 mM	A), B) and C)

1.2 Preparation of the plastic wells microplate

The ELISA-like plastic wells were purchased from Sigma-Aldrich. In a typical preparation, 200 μl of a solution containing the dicopper azacryptate and 6-TAMRA (12 μM and 0.12 μM,

respectively, in water:methanol 1:1 v:v mixture) were dropped on ~100 mg of SiO_2 (for chromatography, 63 μm) into each well (24 wells in total, see black triangles in Figure 5). Each well contained 2.3 nmol of $[Cu_2\mathbf{L}]^{4+}$ and 0.23 nmol of 6-TAMRA. The solutions were then evaporated in dark (the water:methanol mixture was chosen to accelerate the evaporation process). For the construction of the calibration curve shown in the manuscript, Fig. 5, fixed volumes (150 μl) of buffered aqueous solutions containing increasing amounts of **tt-MA** (0.05M HEPES, pH 7) were added to the wells. After addition, the microplate was exposed to a UV lamp (366 nm, 16W), see 1.5 for the determination of RGB indexes.

1.3 Pretreatment of the real urine samples

Before analysis, urine samples were pretreated following the procedure proposed by Bahrami et al.,[2] consisting in a micro-extraction by packed sorbent (MEPS).

This procedure has several advantages: removal of neutral and cationic interferents; extraction and preconcentration of the anionic components (i.e. the analyte and other anions).

For the preparation of SAX cartridges, ~20 mg of quaternary ammonium exchange resin (SAX) were packed between two polyethylene frits inside a 1 mL plastic syringe. After sorbent conditioning (3 x 500 μl MeOH followed by 3 x 500 μl water), the urine sample (either blank or spiked with **tt-MA**) was passed through the sorbent (4 x 500 μl). The sorbent was then washed with water (3 x 500 μl). The anionic components of urine were eluted with 500 μl of 10% (v:v) acetic acid. The eluate was then taken to dryness and the residue was re-dissolved in 500 μl of 0.05 M HEPES pH 7. The analyte concentration in the final solution is 4X.

1.4 Determination of the RGB indexes

The microplate was exposed to the light of a UV lamp (366 nm, 16W) in a dark room. As detector we used a smartphone Samsung S6, provided with the ColorMeter Free App. The smartphone camera was placed in front of the microplate (distance = 15 cm) and the digital image of each well was taken under UV illumination in a dark room. The RGB values were recorded, and the calibration curve was obtained by plotting the RGB indexes vs. analyte concentration in the wells. We chose to monitor the R index since it was the one which showed significant change with the analyte concentration. A good correlation was found between the normalized R index (i.e. R/R_0) and mg L^{-1} of tt-MA (see Fig. 5 in the manuscript). LOD and LOQ parameters were obtained from the calibration curve shown in Section 5, Fig. S7. The experiments with standard tt-MA solutions

and real samples were repeated three times, with three repetitions each. The % recovery was obtained by dividing the averaged R indexes recorded with real samples by the indexes determined with standard solutions (x 100). The results are shown in Section 5, Table S3.

1.5 Computational study

All the calculations were carried out using the GAUSSIAN09 program package.[3] The structures were optimised in the triplet spin state at the UB3LYP/6-31G(d) level for all atoms, except Cu for which the effective core potential LanL2DZ was used. All the optimization were performed in water as solvent, using the classical polarizable continuum model (PCM). Vibrational frequencies were computed at the same level of theory to define the optimized structures as minima, showing all positive frequencies. When optimised at a higher level (6-311+G(d,p) for C,H, N, O and LanL2DZ for Cu) almost identical geometries were obtained with similar energy differences among the conformers.

2. DFT calculations

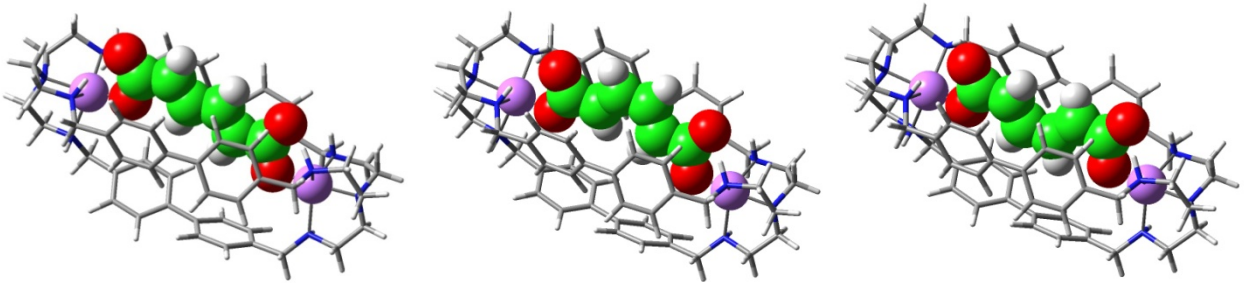

Figure S1. Three-dimensional plots of the preferred conformers of the $[Cu_2\mathbf{L}(\text{tt-MA})]^{2+}$ complex. Cu(II) ions are represented as pink spheres. Different colour codes have been applied for carbon atoms, in order to differentiate receptor and guest carbon skeletons and better visualise the conformation assumed by t,t-MA inside the cavity (e.g. C of the guest: green; C of the receptor: grey).

Table S2. Relative energy and selected geometrical features of the preferred conformers of the $[Cu_2\mathbf{L}(tt\text{-}MA)]^{2+}$ complex (optimized at the B3LYP/6-311+G(d,p) level for C, H, N, O and LanL2DZ for Cu).

	E_{rel} (kcal/mol)	copper-copper distance (Å)	coordinated oxygen atoms distance (Å)	Muconate C2-C3-C4-C5 torsional angle (°)
Muconate-A	0.00	10.78	7.03	176
Muconate-B	2.34	10.72	6.89	-19
Muconate-C	2.54	10.77	6.92	-19

3. Studies with tt-MA

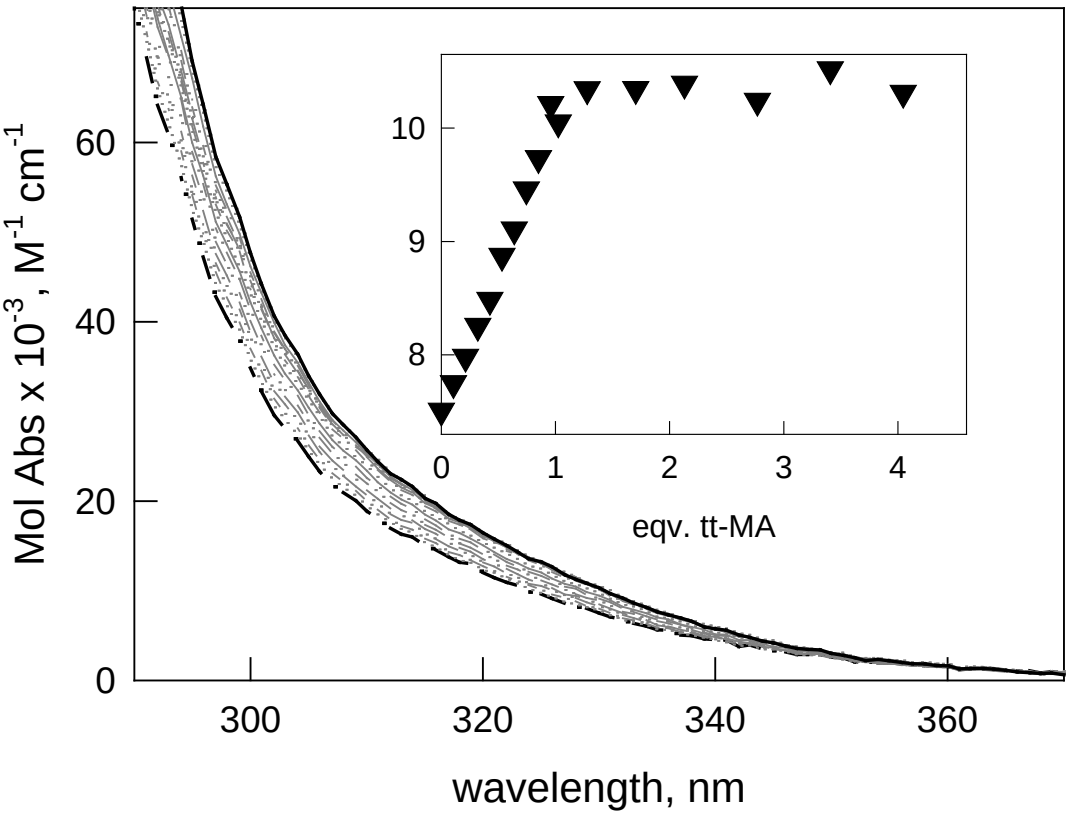

Figure S2: UV-vis. titration of a 8.7 μM solution of $[Cu_2\mathbf{L}]^{4+}$ with tt-MA (HEPES 0.05 M, pH 7; path length = 1cm): family of spectra as Mol Abs x 10^{-3} vs. wavelength. Inset: profile of Mol Abs x 10^{-3} at 330 nm vs. eqv. ttMA

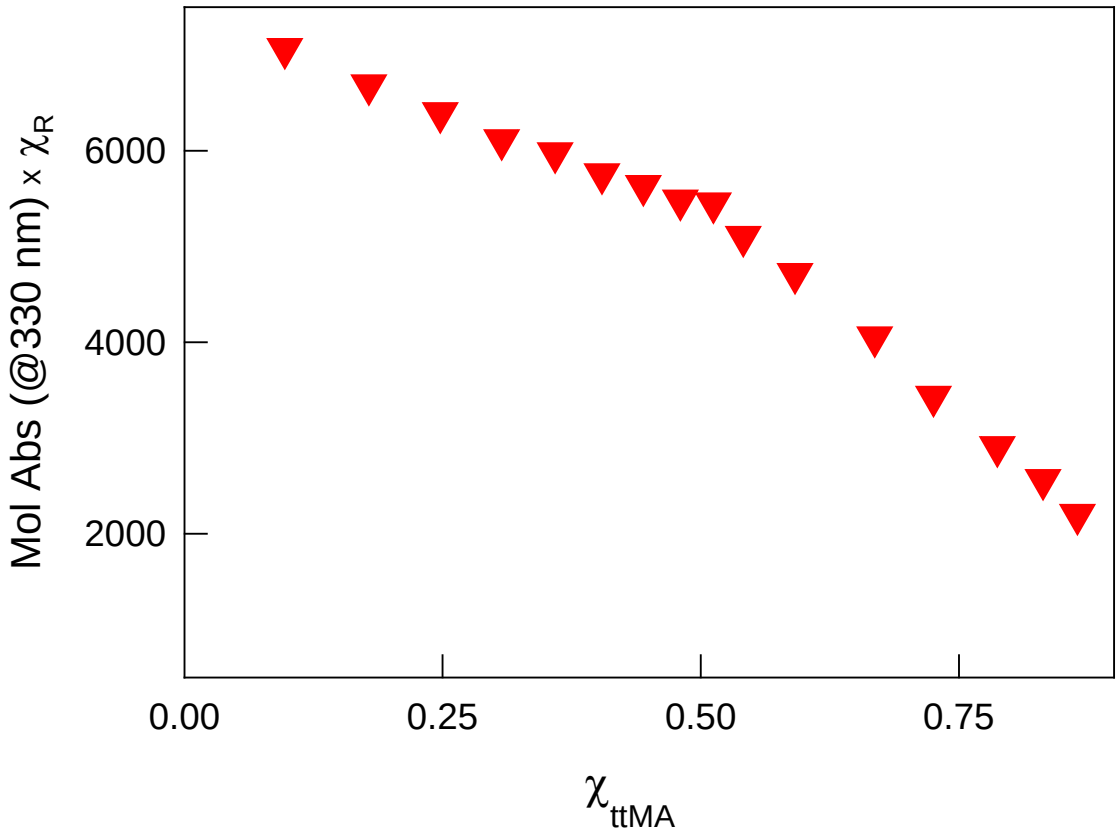

Figure S3: Job plot at 330 nm, corresponding to the profile shown in Figure S2.

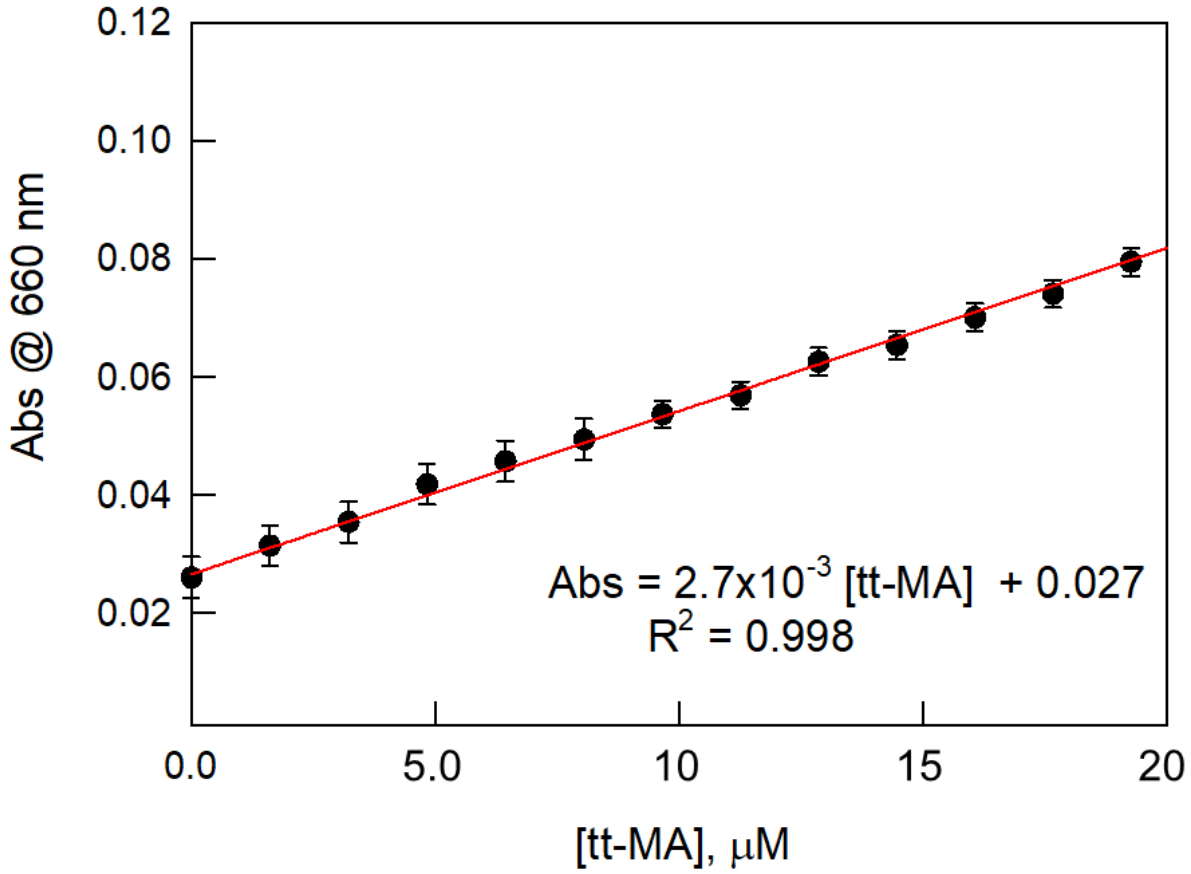

Figure S4: tt-MA calibration curve (red line: fitting curve; dots: experimental data), obtained from the UV-vis titrations of $[Cu_2\mathbf{L}]^{4+}$ (20 μM) with tt-MA (HEPES 0.05 M, pH 7, path length=10 cm). The plotted parameters are linearly correlated for Abs values between 0.027 and 0.080 (R^2 = 0.998).[4] Data are averages of n = 3; error bars represent s.d..

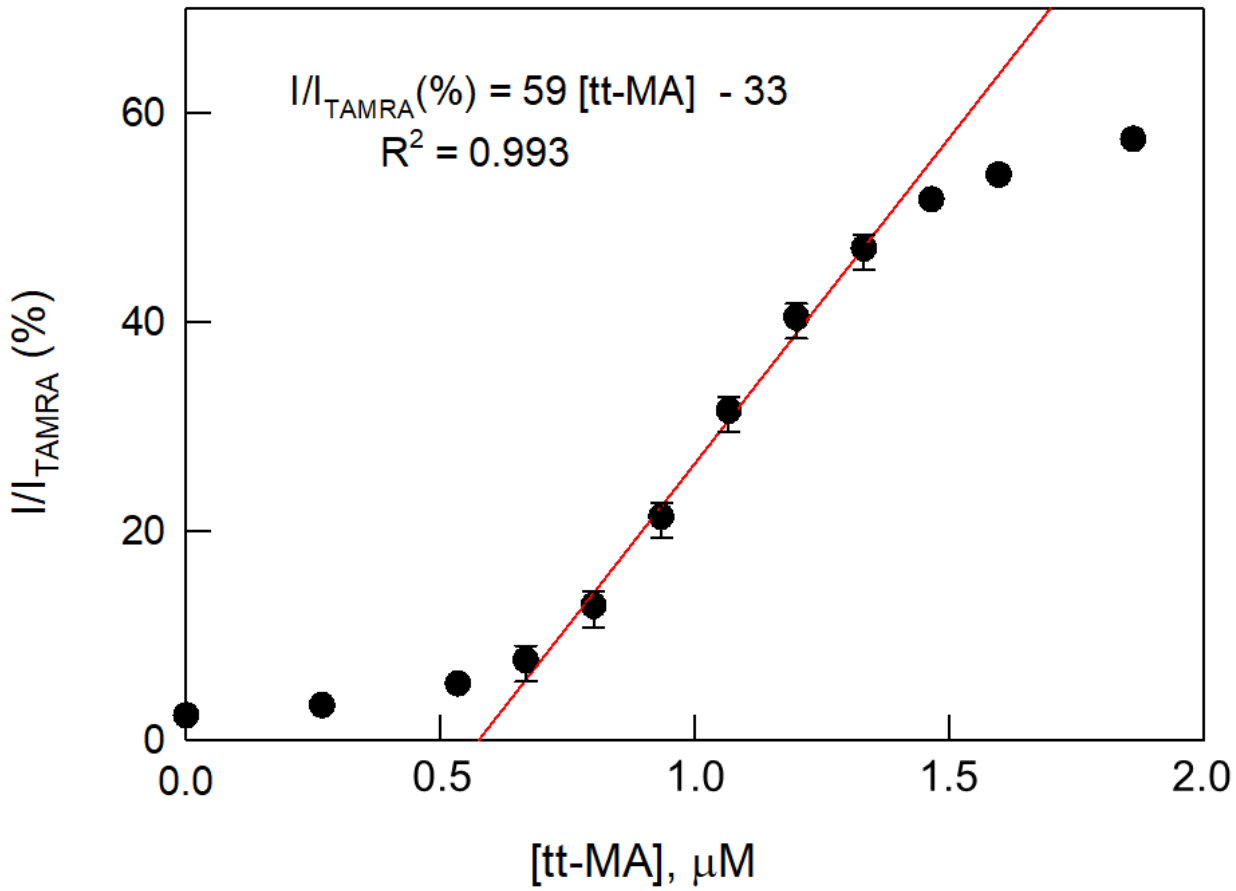

Figure S5: tt-MA calibration curve[5] (red line: fitting curve; dots: experimental data), obtained from the fluorimetric titrations of the chemosensing ensemble solution (1.5 μM $[Cu_2\mathbf{L}]^{4+}$ and 0.2 μM 6-TAMRA, λ_{exc} = 520 nm) with tt-MA (HEPES 0.05 M, pH 7, path length=1 cm). I_{TAMRA} = fluorescence intensity of a 0.2 μM 6-TAMRA solution (recorded before the addition of $[Cu_2\mathbf{L}]^{4+}$) in 0.05 M HEPES at pH 7. The plotted parameters are linearly correlated when I/I_{TAMRA} is between ~10% and 50% (R^2 = 0.993). Data are averages of n = 4; error bars represent s.d.

4. Studies with possible competitors

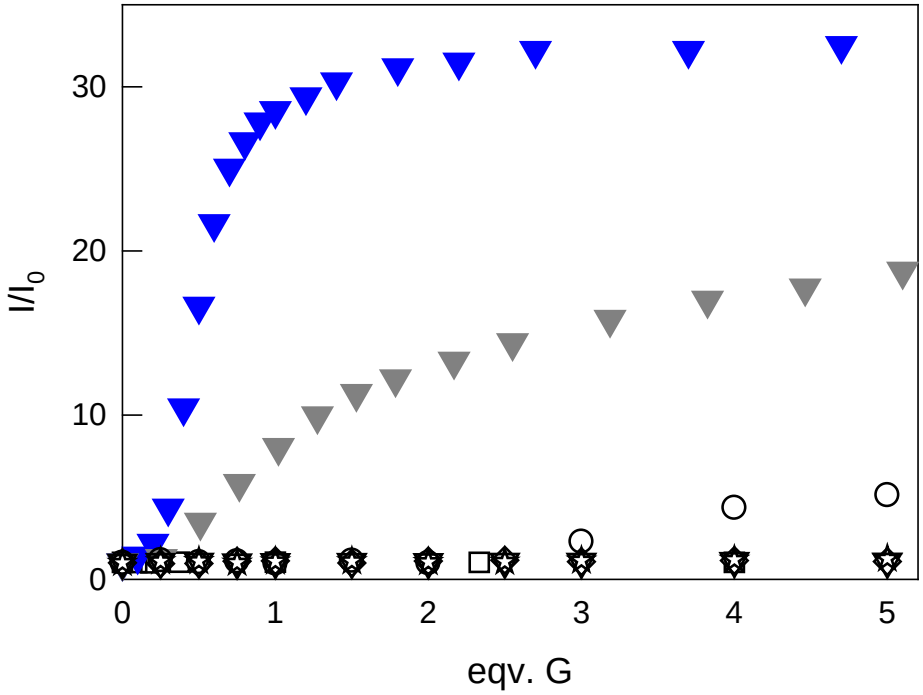

Figure S6: Profiles of the fluorescence intensity (in arbitrary units, a.u.) at 574 nm vs. equivalents of the added guest (G), obtained under fluorimetric titrations of the chemosensing ensemble solution (1.5 μM $[Cu_2\mathbf{L}]^{4+}$ and 0.2 μM 6-TAMRA in HEPES 0.05 M, pH 7; λ_{exc} = 520 nm path length=1 cm) with a series of dioic acids: t,t-MA (blue triangles), adipic acid (grey triangles), maleic acid, fumaric acid, succinic acid, suberic and sebacic acid (white circles, triangles, squares, stars and diamonds, respectively).

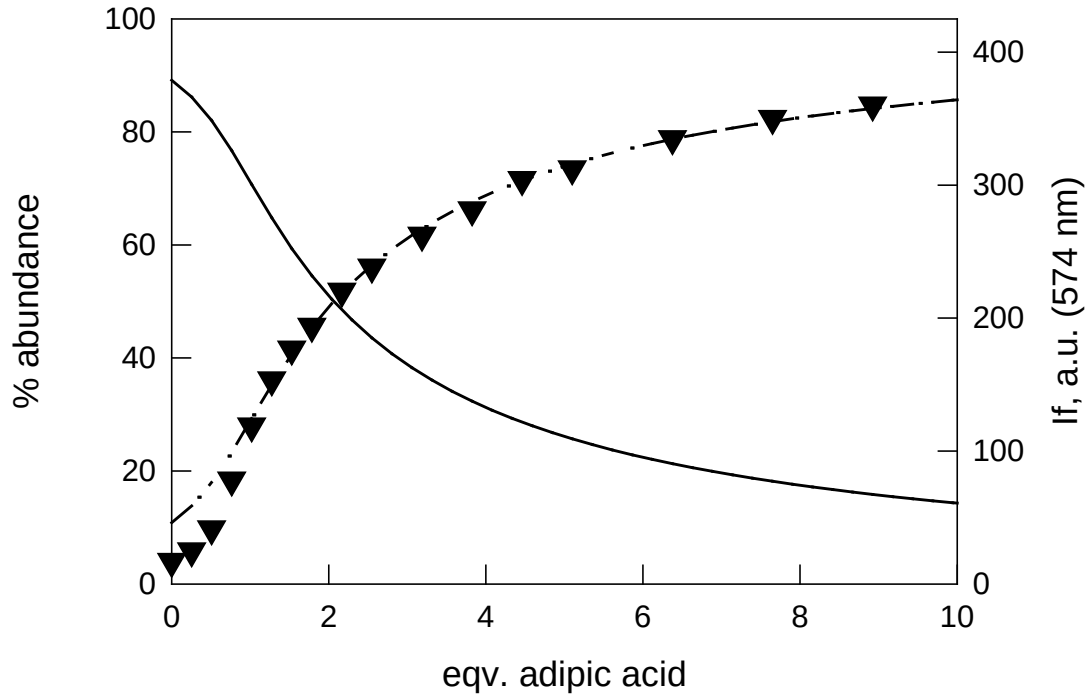

Figure S7: Fluorimetric titration of the chemosensing ensemble solution (1.5 μM $[Cu_2\mathbf{L}]^{4+}$ and 0.2 μM 6-TAMRA, λ_{exc} = 520 nm) with adipic acid (HEPES 0.05 M, pH 7, path length=1 cm). Profile of the fluorescence intensity (in arbitrary units, a.u.) at 574 nm vs. equivalents of the adipic acid (see triangles) with the superimposed distribution diagram of the 6-TAMRA indicator (dashed line: % $[Cu_2\mathbf{L}$(6-TAMRA)$]^{3+}$, solid line: % free 6-TAMRA) vs eqv. anion. The distribution diagram was obtained considering an association constant of 6.9(2) log units (relative to the formation of the 1:1 $[Cu_2\mathbf{L}$(adipate)$]^{2+}$ adduct).

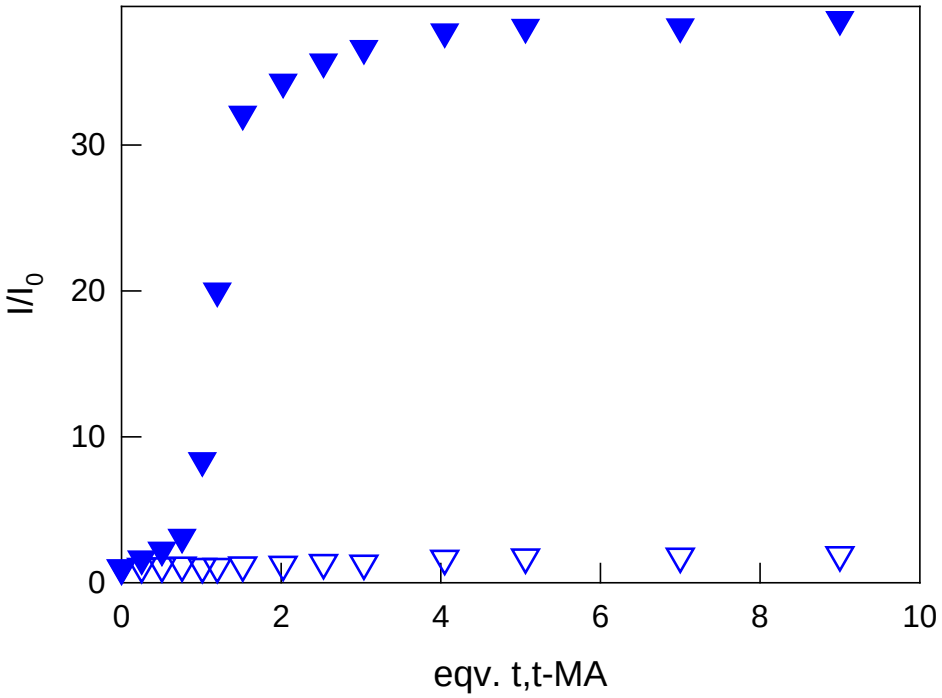

Figure S8: Blue triangles: plot of I/I_0 at 574 nm vs. equivalents of tt-MA obtained under titration of the chemosensing ensemble solution (1.5 μM $[Cu_2\mathbf{L}]^{4+}$ and 0.2 μM 6-TAMRA) in HEPES (0.05M, pH 7) with t,t-MA in artificial urine + 150 ppm HSA. White triangles: profile of I/I_0 at 574 nm for the blank titration (addition of same volumes of artificial urine + 150 ppm HSA, to the chemosensing ensemble solution)

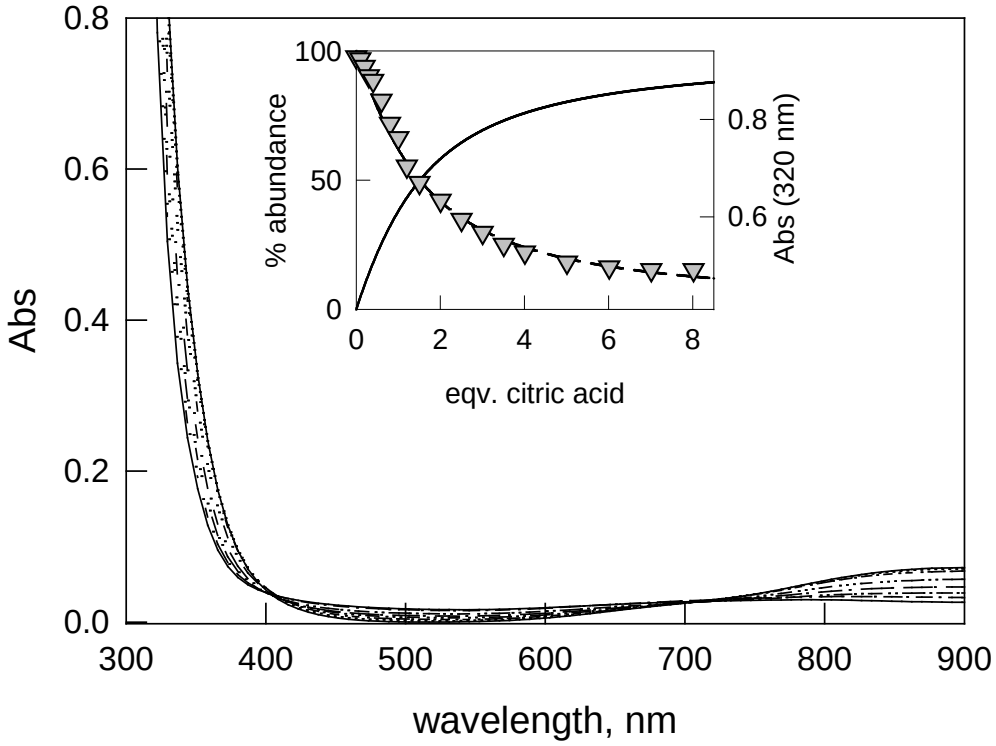

Figure S9: UV-vis. titration of a 20 μM solution of $[Cu_2\mathbf{L}]^{4+}$ with citric acid (HEPES 0.05 M, pH 7, path length=10 cm). Inset: distribution diagram (as % abundance vs. eqv. of the added guest) with the superimposed experimental of the Absorbance at 320 nm. The distributions diagram has been obtained considering a 1:1 equilibrium with a binding constant of 4.7 Log units.

5. Studies in ELISA-type wells microplate

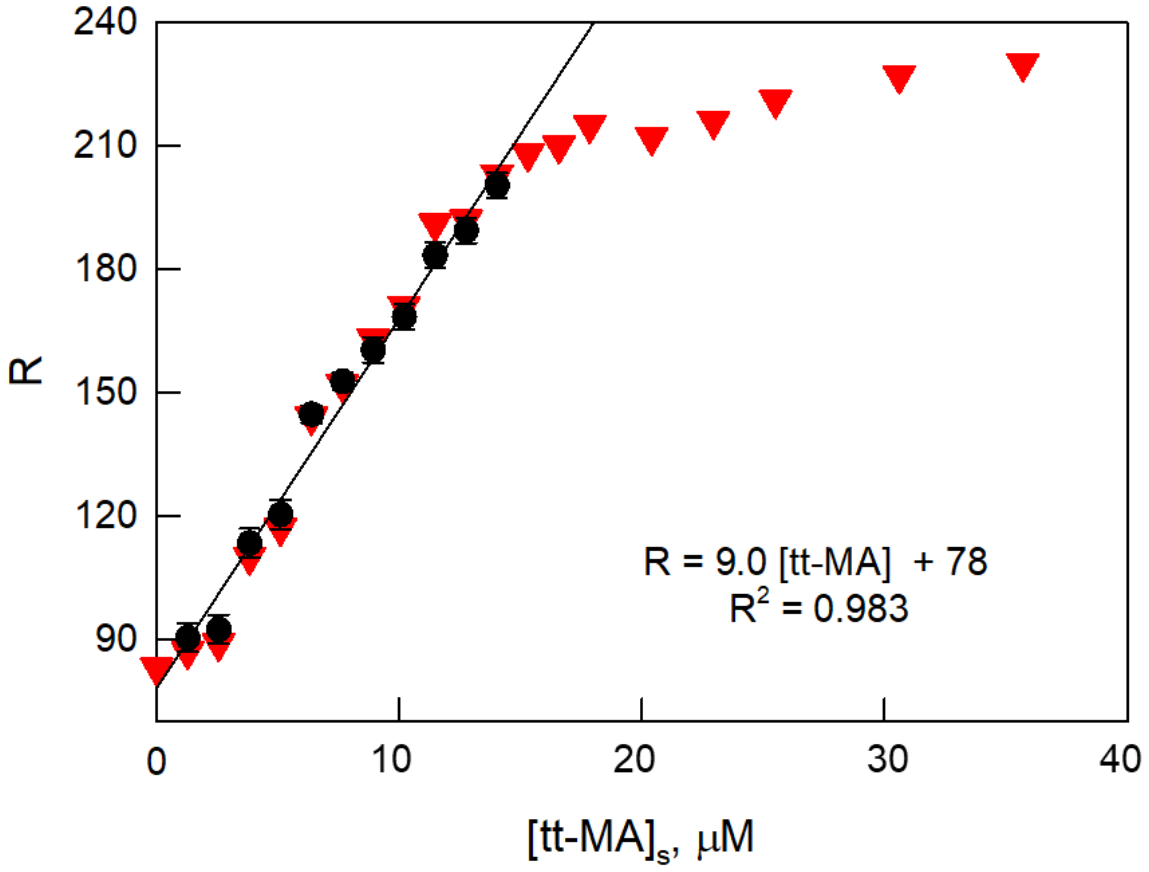

Figure S10: tt-MA calibration curve (black line: fitting curve; dots: R averaged), obtained from the RGB determination in ELISA-type wells. Red symbols correspond to experimental data obtained in one of the trials. Black dots are averages of n = 3 repetitions. The plotted parameters are linearly correlated for R averaged values between 90 and 200 (R^2 = 0.983); error bars represent s.d..

Table S3. For each sample $[tt\text{-}MA]_s$ (obtained by pre-concentration of the initial urine sample, $[tt\text{-}MA]_0$, on SAX cartridge), the **% recovery** was calculated by dividing the averaged R indexes recorded with real samples, $\bar{R}$ **urine**, by the indexes determined with standard solutions, $\bar{R}$ **standard**, x 100. Experiments were repeated at least three times, with three repetitions each.

$[tt\text{-}MA]_0$, M, mg L^{-1}	$[tt\text{-}MA]_s$, M, mg L^{-1}	$\bar{R}$ urine	$\bar{R}$ standard	% recovery
1.25×10^{-6}, 0.18	5.01×10^{-6}, 0.71	117.7	120.1	98.0
2.55×10^{-6}, 0.36	1.02×10^{-5}, 1.4	166.7	168.7	98.7

References

[1] T. Brooks and C.W. Keevel, *Lett. Appl. Microbiol.*, 1997, **24**, 203.

[2] E. Soleimani, A. Bahrami, A. Afkhami, F. G. Shahna, *Toxicol. Environ. Health Sci*., 2017, **9**, 317.

[3] M. J. Frisch, G. W. Trucks, H. B. Schlegel, G. E. Scuseria, M. A. Robb, J. R. Cheeseman, G. Scalmani, V. Barone, B. Mennucci, G. A. Petersson, H. Nakatsuji, M. Caricato, X. Li, H. P. Hratchian, A. F. Izmaylov, J. Bloino, G. Zheng, J. L. Sonnenberg, M. Hada, M. Ehara, K. Toyota, R. Fukuda, J. Hasegawa, M. Ishida, T. Nakajima, Y. Honda, O. Kitao, H. Nakai, T. Vreven, J. A. Jr. Montgomery, J. E. Peralta, F. Ogliaro, M. Bearpark, J. J. Heyd, E. Brothers, K. N. Kudin, V. N. Staroverov, T. Keith, R. Kobayashi, J. Normand, K. Raghavachari, A. Rendell, J. C. Burant, S. S. Iyengar, J. Tomasi, M. Cossi, N. Rega, J. M. Millam, M. Klene, J. E. Knox, J. B. Cross, V. Bakken, C. Adamo, J. Jaramillo, R. Gomperts, R. E. Stratmann, O. Yazyev, A. J. Austin, R. Cammi, C. Pomelli, J. W. Ochterski, R. L. Martin, K. Morokuma, V. G. Zakrzewski, G. A. Voth, P. Salvador, J. J. Dannenberg, S. Dapprich, A. D. Daniels, O. Farkas, J. B. Foresman, J. V. Ortiz, J. Cioslowski and D. J. Fox, Gaussian 09, Revision D.01, Gaussian, Inc., Wallingford, CT, 2010.

[4] R. Rajmohan, K. B. A. Ahmed, S. Sangeetha, V. Anbazhagan and P. Vairaprakash, *Analyst*, 2017, **142**, 3346.

[5] L. Saleh and C. Plieth, *Nat. protoc*., 2010, **5**, 1635.